A&A 375, 1032–1039 (2001)
DOI: 10.1051/0004-6361:20010900

Astronomy & Astrophysics

Pulsar bow-shock nebulae

I. Physical regimes and detectability conditions

N. Bucciantini[1] and R. Bandiera[2]

[1] Dip. di Astronomia e Scienza dello Spazio, Università di Firenze, Largo E. Fermi 5, 50125 Firenze, Italy
e-mail: niccolo@arcetri.astro.it
[2] Osservatorio Astrofisico di Arcetri, Largo E. Fermi 5, 50125 Firenze, Italy

Received 23 May 2001 / Accepted 20 June 2001

Abstract. Pulsar bow-shock nebulae originate from the interaction of the ambient medium with the wind of a moving pulsar. The properties of these nebulae depend on both the physical conditions in the ambient medium and the characteristics of the pulsar wind, and may thus represent a powerful diagnostic tool. The main limits to this study are, on the observational side, the very limited sample of pulsar bow-shock nebulae known so far and, on the theoretical one, a still limited understanding of the physical conditions in these nebulae: in particular, classical bow-shock models are not appropriate to describe these objects. In this paper we outline the most likely physical regimes for nebulae associated with typical pulsars, and discuss why classical models cannot be applied to these objects. We also discuss how microphysical processes may affect both the dynamics of the flow and the properties of the emission (mostly in Balmer lines). We finally put forward a criterion to select among the known pulsars those with the highest probability of having a detectable bow-shock nebula.

Key words. shock waves – stars: pulsars: general – stars: winds, outflows – ISM: general

1. Introduction

When a pulsar moves through the ambient medium, the wind of the pulsar interacts with it, eventually forming a steady flow, with a bow shock in the direction of the stellar motion. The ambient medium can either be interstellar medium (ISM), or belong to the supernova remnant originated at the same time of the pulsar. The latter case is not suited for a detailed, quantitative modelling, because the density and velocity pattern in a supernova remnant may be very complicate, and variable with time. The former one, instead, is in principle a much cleaner case, because the ISM component is seen by the pulsar as a plane-parallel flow, likely with a constant density (at least on the typical scale length of the bow shock), and lasting long enough to allow a steady-state regime. The characteristics of this bow shock may therefore represent a potential diagnostic tool on the medium as well on the pulsar wind. There are however complications both on the theoretical and on the observational side.

In fact no realistic model has been put forward yet, describing in detail the physics involved in the interaction between the pulsar wind and the ISM. Classical bow-shock models are often used (e.g. thin-layer approximation; Wilkin 1996), although some of the classical assumptions (like non-relativistic, non-magnetized, radiative fluid) do not usually apply to the case of pulsar bow-shock nebulae. It is in fact well known that the pulsar wind is relativistic and magnetized, that the ISM is typically partly neutral, and that the neutral atoms may have collisional mean free paths comparable with the scale length of the system, then invalidating a pure fluid assumption. In addition to the intrinsic difficulty in modelling all these effects, a preliminary problem is understanding which of them are important, and how do they contribute to the observed bow-shock properties: this can only be accomplished by a close comparison between models and observations.

However, out of above one thousand radio pulsars known, associated bow shocks have been discovered just in very few cases. While synchrotron emission from the relativistic material in the wind seems too weak to make these nebulae detectable (Gaensler et al. 2000), the emission of optical Balmer lines (mostly Hα) is more relevant. It is the signature of a non-radiative shock moving through a partially neutral medium (Chevalier & Raymond 1980), and originates from de-excitations of neutral H atoms, following collisional excitations or exciting charge-exchange processes. It dominates the optical emission when recombination times are long, and it has been

Send offprint requests to: R. Bandiera,
e-mail: bandiera@arcetri.astro.it

extensively studied on various supernova remnants (Smith et al. 1991). However only four Balmer bow-shock nebulae associated with pulsars are known so far: PSR 1957+20 (Kulkarni & Hester 1988), PSR 2224+65 (Cordes et al. 1993), PSR J0437+4715 (Bell 1995), and PSR 0740–28 (Jones et al. 2001); while it is not clear yet whether the cometary-like nebula associated with the isolated neutron star RX J185635–3754 (van Kerkwijk, ESO press-release 19/00) is resulting from a bow shock.

A puzzling point is why only two out of the four nebulae known present a shape closely matching that of a classical bow shock. The nebula associated with PSR 2224+65 shows a more peculiar shape (which justifies why it has been named "Guitar Nebula"), with a remarkably conical tip (Cordes 1996): is this shape the effect of a peculiar ISM density distribution in the surroundings of the PSR 2224+65 (Cordes et al. 1993), or is it telling us that standard bow-shock models are not adequate for this class of objects? The fourth nebula, which has been lately discovered (Jones et al. 2001) near PSR 0740–28, seems to represent an intermediate case, with a "standard" head but with an unexpectedly conical tail.

Goal of this paper is to investigate the space of physical parameters, typical for known pulsars, and outline the most likely regimes for the flow. We intend to throw a bridge between what could be modelled and what could be observed, by using a simple analytic approach, which allows us to derive the physical conditions in the bow-shock head.

The plan of the paper is as follows: in Sect. 2 we present results on the hydrodynamics in a bow-shock head, that will be used in rest of the paper; Sect. 3 discusses effects of the microphysical processes on the evolution of the neutral H atoms; in Sect. 4 we analyze which physical regimes are appropriate for known pulsars; the effects on the Hα emission are presented in Sect. 5; finally, the discussion presented in Sect. 6 is focused on the selection criteria that should be used in searches for new such objects, and on the requirements for successfully modelling these objects.

2. Hydrodynamics in the bow-shock head

If we neglect the possible onset of turbulent motions, and assume that the hydrodynamic motions are all laminar, the space can be subdivided into 4 regions that, from the outside towards the star, are respectively filled by: unshocked ambient medium (labelled as UA); shocked ambient medium (SA); shocked stellar wind (SW); unshocked wind (UW). The regions are separated respectively by: an outer shock (hereafter referred to as OS), between UA and SA; a contact discontinuity, between SA and SW; an inner shock, between SW and UW. In this paper we shall consider only the head of the bow shock, by approximating the surfaces with planes. If the pulsar wind is nearly isotropic the flows in regions UA and UW are orthogonal to these planes, and the overall flow is axially symmetric. A stagnation point (hereafter SP) is located on the intersection of the contact discontinuity with the symmetry axis, at a distance $d_{\rm o}$ from the star.

A necessary condition for the formation of a bow shock is that the pulsar moves supersonically with respect to the ambient medium: this is the case for most pulsars, with typical velocities $V_{\rm o} \gtrsim 100\,{\rm km\,s^{-1}}$ corresponding, for a 10^4 K ISM, to a Mach number of the ISM flow $M_{\rm o} \gtrsim 10$. A requirement for the existence of a Balmer-emitting nebula is a partially neutral medium, and therefore the case of a hot ISM will not be treated here. Since in the Rankine-Hugoniot relations the corrections for finite $M_{\rm o}$ are of order of $M_{\rm o}^{-2}$, at the OS the fluid quantities can be evaluated with good accuracy even neglecting these corrections.

If the injection of mass, momentum and energy inside the region are negligible, both the Bernoulli ($\mathcal{B}$) and the entropy ($\mathcal{S}$) term are constant along fluid lines:

$$\mathcal{B} = \frac{V^2}{2} + \frac{5}{2}\frac{P}{\rho} = \frac{V_{\rm o}^2}{2}, \tag{1}$$

$$\mathcal{S} = \frac{P}{\rho^{5/3}} = \frac{3}{4^{8/3}}\frac{V_{\rm o}^2}{\rho_{\rm o}^{2/3}} \tag{2}$$

(where we have used $\gamma = 5/3$). This allows us to write density and pressure in terms of the velocity modulus:

$$\frac{\rho}{\rho_{\rm o}} = 4\left(\frac{16}{15}\left(1 - \frac{V^2}{V_{\rm o}^2}\right)\right)^{3/2}, \tag{3}$$

$$\frac{P}{\rho_{\rm o} V_{\rm o}^2} = \frac{3}{4}\left(\frac{16}{15}\left(1 - \frac{V^2}{V_{\rm o}^2}\right)\right)^{5/2}, \tag{4}$$

with V ranging from $V_{\rm o}/4$ down to zero.

At the SP, where V vanishes, density and temperature then reach their maximum value:

$$\rho_{\rm SP} = 1.102\,\rho_{\rm OS}, \qquad T_{\rm SP} = 1.066\,T_{\rm OS}, \tag{5}$$

which, in both cases, is close to the post-shock one. This implies that spatial variations of ρ and T in the head are rather mild: in the following their "typical" values near the head will be simply approximated by their values right behind the outer shock. In the evaluation of average collision rates, we shall also approximate the velocity profile by a linear interpolation between its value at the OS and that at the SP.

The pulsar wind is expected to be relativistic and magnetized: the plasma in the shocked wind is then very light, and does not cool efficiently. For typical conditions, also in the shocked ISM region the probability for an ion to recombine within a flow time ($\sim d_{\rm o}/V_{\rm o}$) is extremely low. Therefore radiative losses are negligible and the "thin-layer approximation", that allows an analytic solution for the flow (Wilkin 1996), is not appropriate here. Wilkin also assumes a complete mixing between the two shocked flows, while formulae appropriate for a laminar flow are given by Chen et al. (1996). A numerical code is required for a complete description of the flow, to compute the thickness of this layer (Δ), as well as its distance from the star.

The standard formula for the distance of the SP,

$$d_{\rm o} = \sqrt{\mathcal{L}/4\pi c\rho_{\rm o}V_{\rm o}^2}, \tag{6}$$

based on the momentum balance and valid in the thin-layer approximation, must now be taken just as an approximated value. Beyond that, we shall see in Sect. 4 that only the fraction of the mass dragged by the SA layer counts.

Using the thin-shock approximation for the surface density $(5\rho_{\rm o}d_{\rm o}/4)$ (Chen et al. 1996), a fair estimate is obtained for the thickness of Region SA,

$$\Delta \simeq \frac{5}{16}d_{\rm o}, \tag{7}$$

confirming that the shock cannot be treated as geometrically thin.

3. Microphysical processes

Consistently with the assumption of laminar flows, we have assumed that ISM and wind material do not mix together "in a fluid sense". However neutral atoms of the ISM are not affected by the (collisionless) OS and penetrate freely in Region SA (and in some cases even beyond it), until they experience collisional interactions with background particles.

In the next sections we shall investigate how much the microphysics may affect the hydrodynamics and the emissivity of the bow shock, and hence the observable properties of the bow shock. Momentum and energy of the originally neutral H atoms is transferred to the plasma, and therefore source terms should be included in the equations describing the evolution of the flow. Moreover the efficiency of the (Balmer-line) emission depends on how many times a H atom reaches an excited state, before it is eventually ionized (under typical conditions recombination processes are inefficient).

Some of the parameters derived by an analysis of the microphysics which enter in the macroscopic description of Region SA are: (1) the fraction of ISM atoms dragged in this region ($X_{\rm drag}$); this quantity affects the size of the bow shock since, in Eq. (6), $\rho_{\rm o}$ must be substituted by $X_{\rm drag}\rho_{\rm o}$; (2) the fraction of ISM ions in this region ($X_{\rm ion}$), which enters in the evaluation of the radiative emission; (3) the Hα efficiency per atom (η). In this section we show how to estimate the quantities $X_{\rm ion}$ and $X_{\rm drag}$: in Sect. 4 they will be used to identify different regimes for the bow-shock hydrodynamics; while in Sect. 5 they will allow us to estimate the nebular emission.

Both in the evaluation and in the use of the above quantities we shall adopt a "one-zone" approximation. For instance, we evaluate average values across the layer, and we apply the $X_{\rm drag}$ correction to the flow parameters without modifying the hydrodynamic equations themselves (as if the drag effect was confined to a narrow layer right beyond the OS).

When a neutral H atom enters Region SA, the main collisional interactions affecting its kinetic status are ionization and charge-exchange (while neutral-neutral interactions can be neglected). Even if, in a strict sense, in a charge-exchange process the motion of the H nuclei does not change, if we follow the path of the neutral atom before and after the interaction the net effect is like that of an elastic "scattering", and here we shall treat it in that way. Ionizations on the other hand behave as "absorption" events. Due to these analogies, in the following we shall estimate their effects by following an approximated treatment similar to that used for combined absorption and scattering of photons (e.g. Rybicki & Lightman 1979). The main weakness of this approach is that it does not account for effects of the specific geometry of the problem, among which the "bouncing back" to Region UA of part of the incoming neutrals. Anyway the accuracy of this approximation is sufficient for our purposes.

For an H atom let us define as α the inverse of the mean free path for ionization, and as β that for charge exchange. These quantities can be expressed in terms of the respective cross sections as

$$\alpha = n_{\rm i} < \sigma_{\rm chex}V_{\rm r} > /V_{\rm o}; \qquad \beta = n_{\rm i} < \sigma_{\rm ion}V_{\rm r} > /V_{\rm o}, \tag{8}$$

where we indicate by $V_{\rm r}$ the relative velocity between the neutral H and a background ion, and by $n_{\rm i}$ the density of ions. Following the notation of Chevalier et al. (1980), we use the suffix s to indicate the first interaction of a neutral, whose velocity with respect to the bow shock is $V_{\rm o}$; we instead use the suffix f for the further interactions of an H atom originated from a charge-exchange event: the two values are different because averaged over different velocity distributions.

For an H atom crossing a slab of material of thickness Δ, we need to estimate the following probabilities: (1) of being ionized at the first interaction ($P_{\rm pure\ ion}$), (2) of being ionized later on ($P_{\rm chex\to ion}$), (3) of leaking after some scattering ($P_{\rm chex\to leak}$), (4) of leaking without any interaction at all ($P_{\rm pure\ leak}$). Numerical simulations are required to estimate these quantities accurately. Here we shall use the following approximate formulae,

$$P_{\rm pure\ ion} = \alpha_{\rm s}(1-\exp(-(\alpha_{\rm s}+\beta_{\rm s})\Delta))/(\alpha_{\rm s}+\beta_{\rm s}); \tag{9}$$

$$\begin{aligned} P_{\rm chex\to ion} &= \beta_{\rm s}(1-\exp(-(\alpha_{\rm s}+\beta_{\rm s})\Delta))/(\alpha_{\rm s}+\beta_{\rm s}) \\ &\times \left(1-\exp(-\sqrt{\alpha_{\rm f}(\alpha_{\rm f}+\beta_{\rm f})}\Delta')\right); \end{aligned} \tag{10}$$

$$\begin{aligned} P_{\rm chex\to leak} &= \beta_{\rm s}(1-\exp(-(\alpha_{\rm s}+\beta_{\rm s})\Delta))/(\alpha_{\rm s}+\beta_{\rm s}) \\ &\times \exp(-\sqrt{\alpha_{\rm f}(\alpha_{\rm f}+\beta_{\rm f})}\Delta'); \end{aligned} \tag{11}$$

$$P_{\rm pure\ leak} = \exp\left(-(\alpha_{\rm s}+\beta_{\rm s})\Delta\right). \tag{12}$$

In the formulae for $P_{\rm chex\to ion}$ and $P_{\rm chex\to leak}$ the former factor indicates the probability that the first event is a charge-exchange process, while the latter factor gives respectively the probability that it is eventually ionized in the slab, or that it escapes from it.

Here Δ' indicates the reduced thickness, after the first interaction, and can be approximated as:

$$\Delta' = \frac{1}{1-\exp(-(\alpha_s+\beta_s)\Delta)} - \frac{1}{\alpha_s+\beta_s}. \quad (13)$$

Although these formulae suffer by strong limitations, they are adequate for our present goals, namely to outline the positions of different regimes in the parameters space, and to estimate the efficiency of Hα emission.

After a H atom leaks through Region SA and penetrates in the (much less dense) Regions SW and UW, the only way of getting ionized is by photons (coming most likely from the pulsar surface). In this case there may be effects on the dynamics of Region SW, but we shall not investigate them in the present work.

The cross sections used in this paper come from Ptak & Stoner (1973) for ionization and from McClure (1966), Newman (1982) and Peek (1966) for charge-exchange.

4. Analysis of the allowed bow-shock regimes

In this section we show how, in a suitable parameters space, one can single out regions corresponding to different physical regimes, allowed for pulsar bow-shock nebulae. We shall refer to the following transitions: (1) between radiative and adiabatic regimes; (2) between efficient and inefficient ionization of the incoming neutrals; (3) between efficient and inefficient drag of the originally neutral component.

Cooling can be neglected when only a minor fraction of the incoming energy flow

$$\Phi_o = X_{drag}\rho_o V_o^3/2 \quad (14)$$

is radiated away. If the cooling rate is defined as $n_e n_p \Lambda(T)$, where $\Lambda(T)$ is the cooling function (Raymond et al. 1976), the adiabaticity condition translates into

$$\frac{\Lambda(T)}{V_o^4} \lesssim \frac{m_H^2}{32\rho_o V_o \Delta}\frac{X_{drag}}{X_{ion}^2}. \quad (15)$$

The use of an equilibrium cooling function when non-equilibrium effects can play a substantial role is generally inappropriate. However, its use here is adequate for our purpose, namely for determining the physical regime of all considered pulsars. As shown in Fig. 1, all pulsars are in the adiabatic regime, and this conclusion is valid even if non-equilibrium effects would enhance $\Lambda(T)$, up to about two orders of magnitude.

Using for $\Lambda(T)$ the temperature at the OS

$$T_{OS} = \frac{3}{32}\frac{m_H V_o^2}{k_B}, \quad (16)$$

the left-side term in Eq. (15) becomes a pure function of V_o. By using Eq. (7) to approximate Δ, and the bow-shock scale (Eq. (6)) corrected for the X_{drag} term,

$$d_o = \sqrt{\mathcal{L}/4\pi c X_{drag}\rho_o V_o^2}, \quad (17)$$

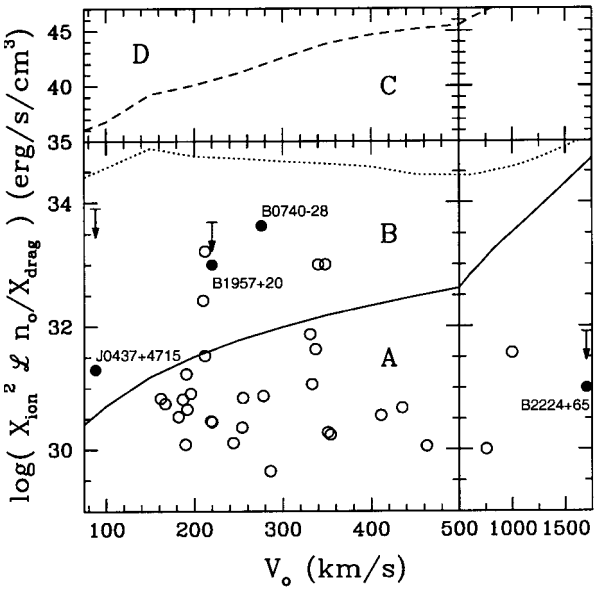

Fig. 1. Positions, in a suitable parameters plane, of the various physical regimes (labelled as A, B, C, D – see text), as well as of some pulsars with known kinematic properties (Cordes & Chernoff 1998). The solid line indicates the transition from leaking to dragged neutral ISM; the dotted line indicates the transition from low to high efficiency in collisional ionization; the dashed line indicates that from low to high radiative efficiency. The circles refer to pulsars parameters derived from their spin-down and kinematic properties, plus a model for the ISM density. Filled circles indicate pulsars with known associated bow-shock nebulae; for three of them upper limits obtained from an analysis of their nebular emission (without using any model for the ISM density or ionization fraction) are also presented.

we finally get the condition

$$\frac{X_{ion}^2\mathcal{L}n_o}{X_{drag}} \lesssim \frac{\pi c m_H^3}{25}\left(\frac{X_{drag}}{X_{ion}}\frac{V_o^4}{\Lambda(V_o)}\right)^2. \quad (18)$$

The condition which separates the adiabatic and radiative regimes is plotted in Fig. 1 (dashed line–the adiabatic regime is below it). This boundary line has been obtained assuming $X_{ion} = X_{drag}$: since in general $X_{ion} \leq X_{drag}$, the line drawn represents the most stringent requirement to guarantee adiabaticity; it is in fact the right condition here, because it happens to lie in a parameters region where both X_{ion} and X_{drag} are close to unity.

The parameters chosen for this plot are V_o and $\xi^2 = X_{ion}^2\mathcal{L}n_o/X_{drag}$. This choice is convenient also in order to define the boundaries of the other physical regimes related to collisional processes: in fact $\xi \propto n_i V_o \Delta$, namely to the product of a collision frequency times the layer thickness. The convenience of using the variables V_o and ξ comes from the fact that in Eqs. (9)–(12) all the arguments of the exponential functions can be re-written as products of ξ times a function of V_o (which can be evaluated on the basis of the appropriate cross section).

From the probabilites given in Eq. (12) one may see that the condition $(\alpha_s+\beta_s)\Delta = 1$ (solid line in Fig. 1)

separates the regime in which neutral atoms can leak through Region SA without any collision (below the line) from that in which charge-exchange and ionization processes cause an effective drag on this component (above the line). The condition $\sqrt{\alpha_{\rm f}(\alpha_{\rm f}+\beta_{\rm f})}\Delta = 1$ (dotted line in Fig. 1), instead, separates the case in which the original neutral fraction is preserved (below the line) from that in which all atoms are eventually ionized (above the line). For the above condition we have used Δ instead of Δ' (like in Eq. (11)): this is justified by the fact that in this region of the parameters plane $(\alpha_{\rm s}+\beta_{\rm s})\Delta \gg 1$ (see Eq. (13)), then leading to $\Delta \simeq \Delta'$.

In Fig. 1 the dividing lines do not cross, and therefore the parameters plane can be subdivided into four distinct regions: A) non-dragging and non-ionizing, B) dragging but non-ionizing, C) dragging and ionizing, D) radiative. A transition from A to D takes place when increasing the ISM density and the pulsar luminosity.

Figure 1 also contains the positions of several pulsars. In order to position a pulsar in the parameters plane we need to know its spin-down luminosity and the velocity with respect to the ambient medium, the density and the ionized fraction of the ambient medium.

The density and ionized fraction of the local ISM have been estimated from models for the Galactic distribution of the neutral component (Dickey & Lockman 1990) and of the ionized one (Taylor & Cordes 1993). Local values may differ considerably from the average ones: anyway the results are only moderately sensitive to the ISM conditions.

We have taken a sample of young pulsars (ages <10 Myr), for which Cordes & Chernoff (1998) estimate the 3-D peculiar velocities. Out of them we have selected those with a motion nearly perpendicular to the line of sight (tilt angle less than ∼30 degres): in this way we did not need to apply corrections for their orientations. We have finally excluded pulsars which are still inside their supernova remnants.

We want to stress that this sample is far from being complete, but it has the advantage of allowing more accurate positions. Using Eqs. (11) and (12), it is possible to evaluate the quantities $X_{\rm drag}$ and $X_{\rm ion}$ for each pulsar, and place it in the parameters plane. The pulsars positions are represented by circles in Fig. 1. The regions, in the parameters plane, which each star belongs to are listed in the second column of Table 1 (for the meaning of the further columns see Sect. 5).

It is apparent that the adiabatic regime is appropriate for all the pulsars we have examined: a radiative bow shock could be formed only if an extremely powerful pulsar is moving through an extremely dense medium, but no such case is known as yet.

For the four pulsars known to have an associated bow-shock nebula (namely PSR J0437–4715, PSR 0740–28, PSR 1957+20, and PSR 2224+65), in Fig. 1 we indicate both the expected positions (filled circles) using the procedure described above, and the upper limits (downward arrow) obtained inferring the ISM conditions directly from the nebular parameters. Since PSR 1957+20 and PSR J0437+4715 were not in the original sample, we have positioned them assuming that their radial velocities are negligible. In the case of PSR 0740–28, for which no quantitative data have been published as yet for the nebula, we have not been able to derive the upper limit. A proof in favour of the effectiveness of the above procedure comes from the agreement between the positions in the plot for all these pulsars, although derived in two different ways.

One may notice that the three cases with a shape of the bow-shock head similar to what expected from a classical model lie in Region B (dragging case); while the Guitar Nebula, exhibiting a peculiar shape, lies in Region A,

Table 1. Pulsar physical regimes and detectability conditions.

Pulsar	Reg	$D/D^A_{\rm lum}$	$D/D^B_{\rm lum}$	$\theta^{\rm a}_{\rm bow}$	$n_{\rm o}$	$X_{\rm o}$
0136+57	*B*	5.8	5.0	0.14	0.17	0.11
0329+54	*A*	8,500	8,200	0.06	0.44	0.095
0355+54	*B*	0.82	0.78	1.0	0.59	0.092
0450+55	*A*	22.6	21.3	1.0	0.39	0.049
0458+46	*A*	190	180	0.24	0.46	0.16
0525+21	*A*	65,000	58,000	0.08	0.11	0.18
0540+23	*B*	6.3	5.1	0.5	0.22	0.31
0611+22	*B*	0.75	0.71	0.77	0.23	0.32
0626+24	*A*	5,900	5,500	0.17	0.067	0.27
0628–28	*A*	21,000	18,000	0.17	0.044	0.35
0630+17	*A*	0.36	0.35	14.3	0.57	0.033
0656+14	*A*	2.7	2.4	2.5	0.37	0.053
0740–28[b]	*B*	0.07	0.06	1.7	0.52	0.17
0823+26	*A*	51	50	1.7	0.17	0.10
0834+06	*A*	520	500	0.7	0.09	0.19
1133+16	*A*	460	320	0.7	0.12	0.14
1426–66	*A*	2,900	2,400	0.18	0.22	0.076
1449–64	*A*	18	16	0.8	0.28	0.060
1508+55	*A*	20,000	7,700	0.45	0.078	0.28
1556–44	*A*	71	68	0.7	0.20	0.088
1749–28	*A*	55	54	0.5	0.57	0.057
1818–04	*A*	560	480	0.25	0.23	0.12
1822–09	*A*	13	12.5	0.9	0.56	0.032
1911–04	*A*	6,800	6,400	0.2	0.068	0.20
1917+00	*A*	15,000	14,000	0.14	0.076	0.18
1929+10	*A*	2.1	2.1	0.2	0.57	0.033
1933+16	*A*	5,300	1,500	0.1	0.095	0.13
1946+35	*A*	41,000	30,000	0.1	0.033	0.26
2020+28	*A*	58	56	0.67	0.38	0.048
2021+51	*A*	120	120	0.67	0.21	0.086
2224+65[b]	*A*	500	120	0.08	0.14	0.13
2351+61	*A*	2,400	1,900	0.1	0.57	0.035

[a] In arcsec; [b] known bow-shock nebula.

namely where neutral atoms can penetrate the internal region of shocked and free-flowing pulsar wind (regions (2) and (1) respectively). How this penetration, and the consequent mass load in the inner regions, may affect the flow and ultimately the shape of the nebula, will be the subject of future investigation. In fact the nebula of PSR 0740–28 shows a "key-hole" shape, with a sort of conical tail: this may represent an intermediate case, in between well-behaving bow shocks and the case the Guitar Nebula.

Concerning the physical size of the bow shock, it is worth noticing that there is no substantial difference between objects in Region A and those in Region B: in our sample, the $d_{\rm o}$ values inferred for pulsars in regime A range from 0.5×10^{15} to 3.0×10^{16} cm, while those for pulsars in regime B range from 6.4×10^{15} to 5.7×10^{16} cm. The average value of $d_{\rm o}$ is larger in regime B due to the higher pulsar luminosity. But this is just a slight effect, because it is dumped by the increase of the dragging efficiency with the bow shock size.

On the observational side, the discovery of a further pulsar bow-shock nebula located in Region A of the parameters plane will be crucial to clarify whether the shape of the Guitar Nebula is caused by a peculiar density distribution in the surrounding medium (Romani et al. 1997) and/or a peculiar pulsar activity, or whether it is a direct consequence of the physical regime.

5. The inferred Hα nebular emission

In this section we estimate the Hα emission from the head of the bow shock in terms of properties of the pulsar (like power and velocity) and of the ISM (like density and ionized fraction).

Near the bow-shock apex the Hα surface luminosity can be written as:

$$\Sigma = \eta (X_{\rm drag} - X_{\rm o}) n_{\rm o} V_{\rm o}, \tag{19}$$

where $X_{\rm o}$ is the original ionized fraction in the ISM , and η is the efficiency in Hα emission, namely the mean number of photons produced per dragged neutral atom (neutrals crossing Region SA without collisions do not emit).

For simplicity let us assume that the pulsar motion is nearly perpendicular to the line of sight. The photon flux per instrumental beam, in the direction of the bow-shock apex, is

$$(\Sigma \theta^2 d_{\rm o}/\tilde{\Delta}) \min(1, \tilde{\Delta}/D\theta) \min(1, d_{\rm o}/D\theta) \tag{20}$$

where θ is the angular resolution, D is the pulsar distance, and $\tilde{\Delta}$ is the thickness of the Hα-emitting layer: in Regime B we have $\tilde{\Delta} \ll \Delta$; for pulsars in Regime A we have $\tilde{\Delta} \simeq \Delta$, but this happens for less powerful pulsars which then produce bow shocks of smaller size. In pratice $\tilde{\Delta}$ is always unresolved, and therefore we shall always use the condition $\tilde{\Delta}/D\theta < 1$. In order to establish a detectability criterion we have used a minimum detectable Hα photon flux per instrumental beam $F_{\rm lim} = F_{\rm o}(\theta/1\,{\rm arcsec})$, where $F_{\rm o} = 4.8 \times 10^{-6}\,{\rm cm^{-2}\,s^{-1}}$: this value is appropriate for a 4-meter telescope with a narrow band filter, an integration time of 1 hour, and a sky background of $\sim$20 mag arcsec^{-2} in the V filter; while cases with different instrumental performances can be easily scaled.

The detectability limit can alternatively be described by defining a limit distance $D_{\rm lum}$ beyond which a given bow shock head cannot be detected. It can be expressed as

$$\frac{D_{\rm lum} X_{\rm ion}}{(X_{\rm drag} - X_{\rm o})} = \left(\frac{d_{\rm o}}{\theta D}\right)^k \frac{\eta}{\sqrt{4\pi c m_{\rm p} F_{\rm o}}} \sqrt{\frac{X_{\rm ion}^2 \mathcal{L} n_{\rm o}}{X_{\rm drag}}}, \tag{21}$$

where: (1) $k = 0$ if the bow shock head is resolved and a detection in each beam is required; (2) $k = 1/2$ if the head is resolved and just a global detection of the head is imposed; (3) $k = 1$ if the head in unresolved. In Fig. 2 we plot the visibility curves for Case 1, while the other criteria can be evaluated only for specific pulsars, Case 2 giving a deeper limit while Case 3 leading to a less deep one. The advantage of a high resolution is evident: it increases the number of spatially resolved bow shocks and allows a deeper limit with respect to that evaluated using the criterion of Case 1.

The efficiency η in the case of $(N+1)$ collisions can be estimated as:

$$\eta = \epsilon \left[\frac{\alpha_{\rm s}}{\alpha_{\rm s}+\beta_{\rm s}} + \frac{\beta_{\rm s}}{\alpha_{\rm s}+\beta_{\rm s}}\left(1 - \left(\frac{\beta_{\rm f}}{\alpha_{\rm f}+\beta_{\rm f}}\right)^N\right)\right] + \frac{g_{\rm eff}\beta_{\rm s}}{\alpha_{\rm s}+\beta_{\rm s}}\left[\frac{\beta_{\rm se}}{\beta_{\rm s}} + \frac{\beta_{\rm fe}}{\alpha_{\rm f}}\left(1 - \left(\frac{\beta_{\rm f}}{\alpha_{\rm f}+\beta_{\rm f}}\right)^N\right)\right], \tag{22}$$

where ϵ is the average number of Hα photons produced per ionization, and is evaluated by using a proportionality between ionization and excitation rates, with a factor varying from $\sim$0.05 for a Ly-α optically thin layer (Case A) to $\sim$0.3 for a Ly-α optically thick one (Case B) (Chevalier et al. 1980). The quantity $g_{\rm eff}$ (Chevalier et al. 1980) is the average number of Hα photons produced per exciting charge-exchange event, namely with an energy above the excitation threshold; while $\beta_{\rm se}$, $\beta_{\rm fe}$ are the rates of these events.

In the regimes of low ionizing efficiency (Regimes A and B of the previous section) η can be written as:

$$\epsilon \left[\frac{\alpha_{\rm s}}{\alpha_{\rm s}+\beta_{\rm s}} + \frac{\beta_{\rm s}\alpha_{\rm f}\beta_{\rm f}}{\alpha_{\rm s}+\beta_{\rm s}}\Delta^2\right] + \frac{g_{\rm eff}\beta_{\rm s}}{\alpha_{\rm s}+\beta_{\rm s}}\left[\frac{\beta_{\rm se}}{\beta_{\rm s}} + \beta_{\rm fe}\beta_{\rm f}\Delta^2\right], \tag{23}$$

where the former term is usually small compared to the latter one: a case with very low efficiency is when the β quantities vanish, because $V_{\rm o}$ is too small ($V_{\rm o} \gtrsim 45\,{\rm km\,s^{-1}}$ is required to avoid this very low efficiency case). In the case of high ionizing efficiency (Regime C of the previous section) we have instead:

$$\epsilon + \frac{g_{\rm eff}\beta_{\rm s}}{\alpha_{\rm s}+\beta_{\rm s}}\left[\frac{\beta_{\rm se}}{\beta_{\rm s}} + \frac{\beta_{\rm fe}}{\alpha_{\rm f}}\right]. \tag{24}$$

Since the transition is rather shallow, we have used an expression changing continuously from the low ionization to the high ionization regime.

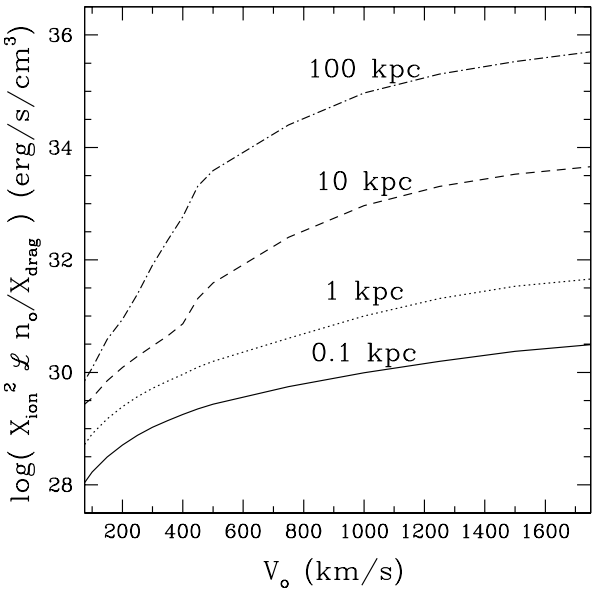

Fig. 2. Visibility curves corresponding to different values of $\tilde{D} = D_{\rm lum} X_{\rm ion}/(X_{\rm drag} - X_{\rm o})$, respectively 0.1 kpc, 1 kpc, 10 kpc, and 100 kpc using a value $\epsilon = 0.1$, an average between the Ly-α thin and thick cases. A pulsar bow-shock nebula should be detected when lying above the relative curve (in Case 1; see text).

In Fig. 2, in the same parameters plane as in Fig. 1, we have drawn the relations between $X_{\rm ion}^2 \mathcal{L} n_{\rm o}/X_{\rm drag}$ and $V_{\rm o}$ for different values of the quantity $\tilde{D} = D_{\rm lum} X_{\rm ion}/(X_{\rm drag} - X_{\rm o})$. The limit distance $D_{\rm lum}$ may be very different from $\tilde{D}$, and can be obtained only after estimating the quantities $X_{\rm ion}$, $X_{\rm drag}$ and $X_{\rm o}$. Individual pulsars can be located in Fig. 2 only after that $X_{\rm ion}$, $X_{\rm drag}$ have been derived (from Eqs. (11), and (12)). In Table 1 we also list the ratio between the actual distance and the maximum allowed distance for detectability of each pulsar in our sample, both for the Ly-α optically thin (Case A) and optically thick (Case B) case. The last three columns give respectively the expected bow-shock angular size (in arcsec), the ISM density (in $\rm cm^{-3}$) and ionization fraction (as derived models of the Galactic distribution; Dickey & Lockman 1990; Taylor & Cordes 1993).

It is apparent that PSR 0740–28 was in fact, among the objects listed here, that with the highest probability to show a Hα bow-shock nebula (i.e. the quantity $D/D_{\rm lum}$ is very small). On the other hand for PSR 2224+65 it seems hard to detect any bow-shock nebula. This result is not contradicted by the fact that a nebula (the Guitar Nebula) has been actually detected: in fact the most prominent part of the nebula is the tail, while the head is very faint and small (0.08 arcsec as "predicted" in Table 1; 0.04 arcsec as actually measured; Cordes et al. 1993). From a comparison with the data our method resulted to have underestimated $D_{\rm lum}$ by a factor $\sim$100: of this, a factor $\sim$10 comes from a local variation of the density with respect to the "average" value obtained by the ISM model we have used; another factor $\sim$10 comes instead from having used, for Table 1, an instrumental resolution of 1 arcsec, while the the resolution of the telescope used (HST, Cordes 1996) is $\sim$20 times higher. As a rule of thumb, there is a chance of detecting a bow-shock nebula in all cases with $D/D_{\rm lum} \lesssim 30$.

6. Discussion

A procedure like that presented above allows one to select, among all pulsars with known timing and kinematic parameters, those most likely associated with a detectable bow-shock nebula: this allows a more focused search for new such nebulae.

The total number of pulsars with known proper motions is much larger than that in the sample we have used here (with 3-D estimates of the velocities, Cordes & Chernoff 1998), but in general no guess is available on their radial velocity component. The above formulae are strictly valid only when a pulsar moves on the plane of the sky; while for tilted velocities the method is less accurate, and tends to overestimate slightly the bow-shock size as well as $D_{\rm lum}$. Anyway a substantial bias would affect only a small fraction of the candidates, and therefore our method can be usually applied also to cases with an unknown tilt.

There are other two corrections that we have not applied here, but which are rather straightforward. First of all, the predicted Hα flux can be corrected for extinction, by assuming a proportionality between the electrons column density toward the source (measured by the pulsar dispersion measure) and the atomic column density (from which the extinction): this relationship is only an approximate one, even though it has been used by various authors (e.g. Romani et al. 1997).

Moreover, the neutron star ionizing emission may affect the ionization fraction of the pre-shocked ISM. A lower limit to the H survival probability to radiative ionization before it reaches the bow shock can be evaluated as

$$\begin{aligned} \mathcal{P} = & \quad \exp\left(- \frac{\pi R_{\rm ns}^2}{V_{\rm o} d_{\rm o}} \int \sigma_{\rm ion} \frac{I(\nu)}{h\nu} \, {\rm d}\nu \right) \\ \simeq & \quad \exp\left(- 0.3 T_6 n_{\rm o} \sqrt{X_{\rm drag}/\mathcal{L}_{33} n_{\rm o}} \right), \end{aligned} \tag{25}$$

where $\mathcal{L}_{33}$ is the pulsar power in units 10^{33} erg s^{-1}, and T_6 is the neutron star temperature in units 10^6 K (assuming a black-body emission from the stellar surface): temperatures $\lesssim 10^6$ K are typical for neutron stars with ages $\sim 10^6$ yr (an upper limit being given by the "standard model"; see Tsuruta 1986), and therefore the effect of stellar ionizing emission is negligible in most cases.

By combining all these pieces we have defined a detectability criterion that will be used in searches for pulsar bow-shock nebulae. The number of candidates will increase considerably in the next few years, when proper motion measurements will become available for recently discovered pulsars: we should not forget that the number

of known radio pulsars has increased by about 100% (Lyne et al. 2000) in the past 5 yr. Once further cases of pulsar bow-shock nebulae will be discovered, one will hopefully be able, by an analysis like that described above, to determine correspondences between properties of the nebula and the physical regime valid for that object.

By now it is suggestive that, out of the four nebulae known, those lying in Region B of Fig. 1 (PSR 1957+20, J0437–4715, and 0740–28) present a bow-shock head with a rather conventional shape, while that lying in Region A (PSR 2224+65) is associated with a nebula with unusual shape (the Guitar Nebula). While this difference has been interpreted (Romani et al. 1997) in terms of a peculiar ISM density distribution, an alternative explanation can be based on the effects of the penetration of neutral ISM atoms in the regions filled by the pulsar wind. It will be very important to find another nebula associated with a pulsar lying in Region A, in order to test the role of the microphysics on the nebular shape.

Also, the tail of PSR 0740–28 nebula deviates from what is expected for a classical bow shock, which makes this object an intermediate case between the Guitar Nebula and the other pulsar bow-shock nebulae. For PSR J0437+4715 there is little chance of seeing a tail, at all, because the stellar velocity, relative to the ISM, is rather low ($\sim 90\,\mathrm{km\,s^{-1}}$) and in the tail, relative atomic velocities are not large enough to allow H excitations. On the other hand PSR 1957+20 and PSR 0740–28 are close to each other, in the parameters plane (Fig. 1): therefore, if the conical tail is a consequence of microphysical processes in the interaction with the ISM, a opening of the tail should be found also in PSR 1957+20. An absence of such effect in PSR 1957+20 would indicate that internal properties on the pulsar wind, like for instance the ratio between magnetic field and particle components, may affect the properties of the bow shock.

In order to investigate in more depth these effects, and to extend the present treatment also to the bow-shock tail, numerical models are under development and the results will be presented in a forthcoming paper.

Acknowledgements. This work has been partly supported by the Italian Ministry for University and Research under Grant Cofin99-02-02, and by the National Science Foundation under Grant No. PHY99-07949.

References

Bell, J. F., Bailes, M., Manchester, R. N., Weisberg, J. M., & Lyne, A. G. 1995, ApJ, 440, L81
Chen, Y., Bandiera, R., & Wang, Z.-R. 1996, ApJ, 469, 715
Chevalier, R. A., & Raymond, J. C. 1978, ApJ, 225, L27
Chevalier, R. A., Raymond, J. C., & Kirshner, R. P. 1980, ApJ, 235, 186
Cordes, J. M. 1996, Pulsars: Problems & Progress, ed. S. Johnston, M. A. Walker, & M. Bailes, ASP Conf. Ser., 105, 393
Cordes, J. M., & Chernoff, D. F. 1998, ApJ, 505, 315
Cordes, J. M., Romani, R. W., & Lundgren, S. C. 1993, Nature, 362, 133
Dickey, J. M., & Lockman, F. J. 1990, ARA&A, 28, 215
Gaensler, B. M., Stappers, B. W., Frail, D. A., et al. 2000, MNRAS, 318, 58
Jones, H., Stappers, B., & Gaensler, B. 2001, The Messenger, 103, 27
Kulkarni, S. R., & Hester, J. J. 1988, Nature, 335, 801
Lyne, A. G., Camilo, F., Manchester, R. N., et al. 2000, MNRAS, 312, 698
McClure, G. W. 1966, Ph. Rv., 148, 47
Newman, J. H., Cogan, J. D., Ziegler, D. L., et al. 1982, Ph. Rv. A, 25, 2976
Peek, J. M. 1966, Ph. Rv., 143, 33
Ptak, R., & Stoner, R. E. 1973, ApJ, 185, 121
Raymond, J. C., Cox, D. P., & Smith, B. W. 1976, ApJ, 204, 290
Romani, R. W., Cordes, J. M., & Yadigaroglu, I.-A. 1997, ApJ, 484, L137
Rybicki, G. B., & Lightman, A. P. 1979, Radiative Process in Astrophysics (John Wiley & Sons, New York)
Smith, R. C., Kirshner, R. P., Blair, W. P., & Winkler, P. F. 1991, ApJ, 375, 652
Taylor, J. H., & Cordes, J. M. 1993, ApJ, 411, 674
Tsuruta, S. 1986, Comm. Ap., 56, 237
Wilkin, F. P. 1996, ApJ, 459, L31